

Inner disc rearrangement revealed by dramatic brightness variations in the young star PV Cep

M. Kun^{1*}, E. Szegedi-Elek¹, A. Moór¹, Á. Kóspál², P. Ábrahám¹,
D. Apai³, Z. T. Kiss¹, P. Klagyivik¹, T. Yu. Magakian⁴, Gy. Mező¹,
T. A. Movsessian⁴, A. Pál¹, M. Rácz¹, J. Rogers³

¹*Konkoly Observatory, Konkoly Thege ut 15-17, H-1121 Budapest, Hungary*

²*Leiden Observatory, Leiden University, Leiden, The Netherlands*

³*Space Telescope Science Institute, 3700 San Martin Drive, Baltimore, MD 21218, USA*

⁴*V. A. Ambartsumian Byurakan Astrophysical Observatory, 0213 Aragatsotn prov., Armenia*

5 November 2018

ABSTRACT

Young Sun-like stars at the beginning of the pre-main sequence (PMS) evolution are surrounded by accretion discs and remnant protostellar envelopes. Photometric and spectroscopic variations of these stars are driven by interactions of the star with the disc. Time scales and wavelength dependence of the variability carry information on the physical mechanisms behind these interactions. We conducted multi-epoch, multi-wavelength study of PV Cep, a strongly variable, accreting PMS star. By combining our own observations from 2004–2010 with archival and literature data, we show that PV Cep started a spectacular fading in 2005, reaching an I_C -band amplitude of 4 mag. Analysis of variation of the optical and infrared fluxes, colour indices, and emission line fluxes suggests that the photometric decline in 2005–2009 resulted from an interplay between variable accretion and circumstellar extinction: since the central luminosity of the system is dominated by accretion, a modest drop in the accretion rate could induce the drastic restructuring of the inner disc. Dust condensation in the inner disc region might have resulted in the enhancement of the circumstellar extinction.

Key words: stars: formation; stars: pre-main sequence; stars: individual: PV Cep

1 INTRODUCTION

Eruptive young stars, defined by their episodically increased optical and infrared brightness, form a small subclass of Sun-like PMS stars. Traditionally they are divided into two groups: FU Orionis type stars (FUors) exhibit an initial brightening of 5 mag during several months or years, followed by a fading phase of up to several decades or a century. The other group, EX Lupi-type stars (EXors) are characterized by relatively short, recurrent outbursts which last some weeks to months, and the time between the eruptions ranges from months to years. In both classes the outbursts are believed to be powered by enhanced accretion from the circumstellar disc on to the star. In the standard picture the inward spiralling material piles up close to the inner edge of the accretion disk, and falls on to the stellar surface as a result of a gravitational and thermal instability (Zhu et al. 2009).

In 2003, the outburst of the low-mass young stellar object V1647 Ori triggered a large number of observations from X-ray to far-infrared wavelengths. Based on these ground-based and space-born measurements it was suggested that this object fits neither into the FUor nor EXor class. It was outlined that the outburst – unlike in other young eruptive stars where enhanced accretion is the main physical driver behind the brightening – consisted of the combination of two effects of comparable amplitude. They are an intrinsic brightening related to the appearance of a new, accretion-related hot component in the system, and a dust-clearing event which reduced the extinction along the line-of-sight (e.g. Acosta-Pulido et al. 2007; Aspin, Beck & Reipurth 2008). The simultaneity of the accretion and extinction changes suggests that they might be physically linked, and the changing accretion luminosity causes changes in the inner disc structure. Another example for such combined processes may be V1184 Tau (Alves et al. 1997) whose optical and infrared photometric observations have shown that the large photometric decline was associ-

* E-mail: kun@konkoly.hu

ated with variation in the inner disc structure (Grinin et al. 2009). That the variable extinction may have an important role in the brightening refines the picture of the FUor/EXor phenomenon, moreover such rearrangements of the inner disc structure have a potentially high importance for the evolution of the terrestrial zone of circumstellar disk.

The target of our multi-wavelength variability study, PV Cep is an eruptive young star, which was originally classified as member of the EXor class by Herbig (1989), on the basis of its large outburst in 1977–1979 (Cohen et al. 1981). Currently the star undergoes significant brightness changes which we have been monitoring for years. Our first observations indicated that PV Cep might be another example for accretion-induced structural changes, and this motivated our further detailed study of the object. The role of variable circumstellar extinction was also apparent in the dramatic brightness decline observed in the near infrared between 2008 April and June by Lorenzetti et al. (2009). Several further observed properties distinguish PV Cep from EXors, and indicate that the object may be more similar in nature to V1647 Ori. Such properties are e.g. the time-scale of the outburst (~ 2 years), the A-type absorption spectrum observed at the beginning of the outburst (Cohen et al. 1981), the Class I spectral energy distribution (SED) (Connelley et al. 2008), the associated high-mass circumstellar disc ($0.76 M_{\odot}$, Hamidouche 2010), variable reflection nebula (Gyulbudaghian & Magakian 1977; Cohen 1980), molecular outflow (Levreault 1984; Arce & Goodman 2002; Hamidouche 2010), and parsec-scale optical jet (Gómez, Whitney & Kenyon 1997; Reipurth, Bally & Devine 1997; Neckel et al. 1987).

We carried out a comprehensive optical and infrared photometric and optical spectroscopic monitoring of PV Cep during the low-brightness state in 2008–2010, and we have a few additional measurements from 2004, 2005, and 2006. In this paper we combine these data with archival and new near- and mid-infrared data, obtained in 2004–2010, to better understand the nature of PV Cep and the nature of physical processes which affect the inner disk structure and evolution.

2 OBSERVATIONS

2.1 Photometry

Photometric observations in the VR_CIC bands spanning the time interval between 2004 September 22 and 2010 November 23 were performed with six instruments on five telescopes. Most of the data were obtained with the 60/90/180 cm Schmidt telescope of the Konkoly Observatory, equipped with a Photometrics AT 200 camera and with the 1-m RCC telescope of the Konkoly Observatory, equipped with a Princeton Instruments VersArray:1300B camera. PV Cep was also observed with the IAC–80 telescope of the Teide Observatory (Spain) between 2009 October 25 and November 7. More detailed description of these instruments is given in Acosta-Pulido et al. (2007). In 2008 August and 2009 October we obtained VRI images with the CAFOS instrument installed on the 2.2 m telescope of the Calar Alto Observatory (Spain). Exposure times were between 90 and 180 s per image. The $I_C = 11.70 \pm 0.04$ magnitude on 2004 September 22 was derived from a CCD-image

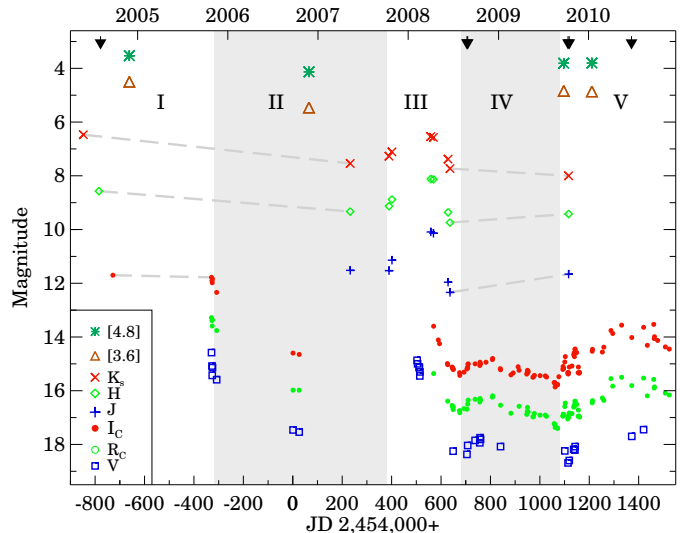


Figure 1. V , R_C , I_C , J , H , K_s , and IRAC [3.6] and [4.8] light curves of PV Cep between 2004 May and 2010 September. V magnitudes in 2008 February were taken from the *INTEGRAL* OMC Archive. Near-infrared data before 2009 are taken from Lorenzetti et al. (2009) and Connelley et al. (2008). The light grey dashed lines, spanning the long time-gaps without data, were drawn to clearly identify the coherent data sets. Arrows indicate the dates of our spectroscopic observations. Roman numbers and shading indicate the five characteristic segments of the light curves.

obtained with the 2.6-m telescope of Byurakan Observatory, Armenia, and shown in the paper of Movsessian et al. (2008). The image of PV Cep was saturated, and its magnitude was derived by fitting the PSF to the unsaturated wing of the stellar image. On 2010 April 8 we used the Electro Multiplying (EM) Andor Technology iXon^{EM} + 888 camera at the RCC telescope of the Konkoly Observatory. We obtained a series of 100 exposures in the I_C band with exposure times of 20 s per image in EM mode (the nominal EM gain was 50). The image processing was made with the software tools written by Pál (2009). All the other images were reduced in IRAF. In order to transform instrumental magnitudes into the standard system, we calibrated 16 stars in the field of view of the 1-m telescope ($7' \times 7'$) in VR_CIC bands. Calibration was made during six photometric nights. Standard stars in NGC 7790, published by Stetson (2000), were used as reference. Equatorial coordinates and derived VR_CIC magnitudes with uncertainties of the comparison stars are listed in Table 1. The results of the photometry for PV Cep are presented in Table 2 and plotted in Fig. 1. The photometric errors were derived from quadratic sums of the formal errors of the instrumental magnitudes and those of the coefficients of the transformation equations. The telescope used for each observation is shown in the last column of Table 2.

2.2 Near-infrared observations

Near-infrared, JHK_s measurements of PV Cep were obtained using the NIC-FPS camera on the ARC 3.5-m Telescope at Apache Point Observatory on 2009 October 12

Table 1. Comparison stars*

N	RA(2000) h m s	D(2000) d ' "	V(ΔV) [mag]	R_C (ΔR_C) [mag]	I_C (ΔI_C) [mag]
C1	20 46 28.89	+67 59 05.4	14.072 (0.012)	13.595 (0.012)	13.200 (0.008)
C2	20 46 26.50	+67 58 11.8	14.608 (0.005)	13.948 (0.004)	13.495 (0.005)
C3	20 46 10.44	+67 55 44.2	15.134 (0.005)	14.205 (0.004)	13.637 (0.004)

*The full Table is available as Supporting Information with the online version of this article.

Table 2. Results of the photometry of PV Cep**

JD (2454000+)	Date yyyymmdd	V(ΔV) [mag]	R_C (ΔR_C) [mag]	I_C (ΔI_C) [mag]	Telescope
-329	20051027	14.58 (0.16)	13.28 (0.06)	11.78 (0.06)	RCC
-327	20051029	15.08 (0.04)	13.39 (0.04)	11.90 (0.11)	RCC
-326	20051030	15.43 (0.06)	13.59 (0.04)	11.98 (0.06)	RCC
-325	20051031	15.14 (0.07)	13.36 (0.01)	11.84 (0.16)	RCC

**The full Table is available as Supporting Information with the online version of this article.

(JD 2455116.5). Dark and domeflat images were also obtained, and four-point dithering was applied to ensure proper sky subtraction. To avoid saturation, the K_s images were slightly defocussed, and, to exclude a nearby bright star from the field of view during the H and K_s exposures, the camera was rotated. The images were reduced in IRAF. Magnitudes were derived by aperture photometry, and were transformed into the standard system by comparing them with the 2MASS magnitudes (Cutri et al. 2003) of four stars in the image field. These stars are as follows: 2MASS 20462889+6759054 (C1 in Table 1), 2MASS 20462650+6758118 (C2), 2MASS 20461044+6755442 (C3), and 2MASS 20461128+6800012. The derived magnitudes are as follows: $J = 11.66 \pm 0.04$, $H = 9.42 \pm 0.04$, $K_s = 8.00 \pm 0.10$.

2.3 Spectroscopy

Intermediate resolution spectra of PV Cep were obtained on 2008 August 26 and 29, 2009 October 9, 11, and 14, using the CAFOS instrument on the 2.2-m telescope of the Calar Alto Observatory. The R-100 grism covered the 5800–9000 Å wavelength range. The spectral resolution of CAFOS, using a 1.5-arcsec slit, was $\lambda/\Delta\lambda \approx 3500$ at $\lambda = 6600$ Å. The spectrum of a He–Ne–Rb lamp was regularly observed for wavelength calibration. Broadband $VR_C I_C$ photometric images were taken immediately before the spectroscopic exposures for flux calibration. We reduced and analysed the spectra using standard IRAF routines. A further R-100 spectrum, obtained on 2004 August 7, and shown in fig. 2 of Kun et al. (2009), is also available.

2.4 Spitzer data

We observed PV Cep using the *Spitzer Space Telescope* between 2004 October and 2005 August with the IRAC, IRS and MIPS instruments. In addition, we used further archival

data from IRAC and MIPS. Moreover, we conducted a monitoring with the IRAC instrument during the post-Helium phase in 2009 September and 2010 January. A log of all Spitzer observations of PV Cep is presented in Table 3. The data reduction procedures are described in Appendix A, available as Supporting Information with the online version of this article. The results of Spitzer photometry are shown in Table 4.

3 RESULTS

3.1 Photometric variations

Light curves of PV Cep in 2004–2010. The light curves of PV Cep in the V , R_C , I_C , J , H , K_s , and IRAC 3.6 and 4.5 μm bands between 2004 May and 2010 November are shown in Fig. 1. Based on the shape of the I_C curve we divided the covered period into five segments, indicated by shading and Roman numbers. The first segment, thereafter referred to as the *bright state*, is the interval between 2004 July and 2005 October. Segment II, the *fading phase*, is the period between 2005 October and 2007 October, when the star faded significantly in each photometric band. Segment III, the *transient peak*, covers the brightening between 2007 October and 2008 February, and the subsequent sharp decline until 2008 June. Segment IV is the *low-brightness state* between 2008 June and 2009 August, when the optical brightness slowly decreased further, reaching a minimum of $I_C = 15.86$ on 2009 August 18. After this date, in segment V, the optical and infrared fluxes, except the K_s -band flux, started rising, and large, short-term brightness fluctuations appeared in the optical light curves. We refer to this interval as the *rising phase*. The total amplitude of the I_C light curve is about 4 magnitudes over the period 2005 November and 2009 September.

Colour–magnitude diagrams. In order to get insight into the origin of the observed variations we plotted colour–

Table 3. Log of *Spitzer* observations of PV Cep

Instrument	Wavelength	Date	AOR	Program
IRAC	3.6, 4.5, 5.7, 8.0 μm	2004 Oct 29	11571712	3716
IRS	5.2 – 37.2 μm	2004 Oct 23	12287488	3716
MIPS SED	55 – 95 μm	2005 Aug 03	11571968	3716
IRAC	3.6, 4.5, 5.7, 8.0 μm	2006 Nov 26	18955008	30760
MIPS	24, 70 μm	2007 Feb 26	19962624, 19962880	30574
IRAC post-He	3.6, 4.5 μm	2009 Sep – 2010 Jan	35591168 – 35678720	60167

Table 4. *Spitzer* photometry for PV Cep. All fluxes are color-corrected and given in Jy^\dagger .

Date	$F_{3.6\mu\text{m}}$	$F_{4.5\mu\text{m}}$	$F_{5.7\mu\text{m}}$	$F_{8.0\mu\text{m}}$	$F_{24\mu\text{m}}$	$F_{70\mu\text{m}}$
20041029	4.47 (0.09)	6.98 (0.14)	8.34 (0.17)	11.85 (0.23)		
20061126	1.84 (0.04)	3.99 (0.08)	5.45 (0.11)	8.16 (0.17)		
20070226					27.12 (1.04)	35.22 (2.13)
20090916	3.54 (0.03)	5.97 (0.02)				

† The full Table is available as Supporting Information with the online version of this article.

magnitude diagrams. Figure 2 (left) shows that the fading in 2005–2006 was nearly grey in the R_C and I_C bands. Its reason may be that in minimum, whatever is the origin of the decline, the star itself is too faint to be detected, only the light scattered from the disc atmosphere, thus bluer in colour, can be observed. The transient peak shows different colour variation: the star became redder and brighter and then bluer and fainter. This colour behaviour is characteristic of UX Orionis (UXor) type variables close to the light curve minima (e.g. Bibo & Thé 1991), and is attributed to the increasing proportion of scattered light when the star is obscured by a circumstellar dust clump. This diagram suggests that the optical source in the dim phases (segments II and IV of the light curve) was the starlight scattered from the disc atmosphere. During the low-brightness phase (filled circles) PV Cep was redder when fainter: this behaviour can result from either enhanced extinction or vanishing hot spots on the stellar surface due to the decreasing accretion rate. In the rising phase the star turned brighter and redder, indicating that instead of the scattered light direct light from the central star could be detected. The data obtained in 2010 indicate that the star completed a full loop in this diagram from 2008 April to 2010 April.

The near-infrared data in Fig. 2 (right) show that the fading in 2005–2006 was accompanied by a slight decrease of the $H - K_s$ colour index, indicative of decreasing emission from the dust sublimation zone of the disc, whereas an extinction change of $A_V \approx 7$ mag can account for the photometric variations around the transient peak in 2008. The different colour behaviour suggests the different nature of the two brightness drops. The strong decrease of the $H - K_s$ colour index at the bottom of the diagram, measured in 2009 October, clearly suggests the fall of the inner disc emission during the low-brightness phase.

Variations in the mid- and far infrared The *Spitzer* data obtained in the bright, fading, and rising phases of the light curve (Table 4) allow us to inspect the wavelength de-

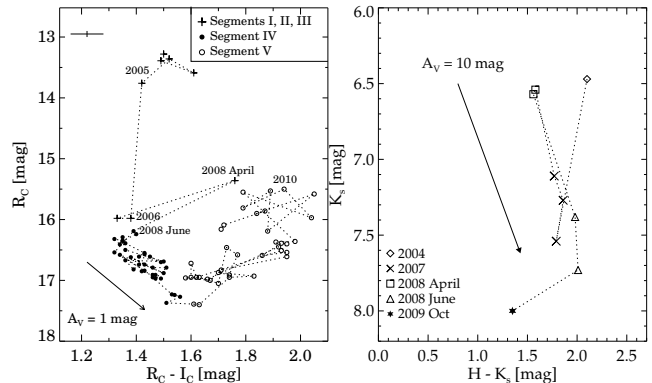


Figure 2. *Left:* R_C magnitude as a function of the $R_C - I_C$ colour index. Consecutive data points are connected by dotted lines. The arrow indicates the colour dependence of the interstellar extinction. The typical error bars are shown in the upper left corner. *Right:* K_s magnitude as a function of the $H - K_s$ colour index based on all data obtained between 2004 and 2010 (Connelley et al. 2008; Lorenzetti et al. 2009). Consecutive data points are connected.

pendence of variations in the mid- and far-infrared regions. We plotted in Fig. 3 the flux ratios between the different segments of the light curve as a function of wavelength. In addition to our own measurements, the bright state data also include H and K_s data from Connelley et al. (2008), and the fading phase data set contains JHK_s data measured on 2007 May 13 (Lorenzetti et al. 2009), as well as the *AKARI IRC* (Ishihara et al. 2010) fluxes at 9 and 18 μm , and *AKARI FIS* catalog data (Yamamura et al. 2010) at 65, 90, 140, and 160 μm , each obtained between 2006 May 8 and 2007 August 26. The wavelength dependence of variations is obviously different from that of the dust extinction: the excess emission in the bright state with respect to fading phase had an optical, a near- and mid-infrared, and a far-infrared component, indicative of changing emission from both the

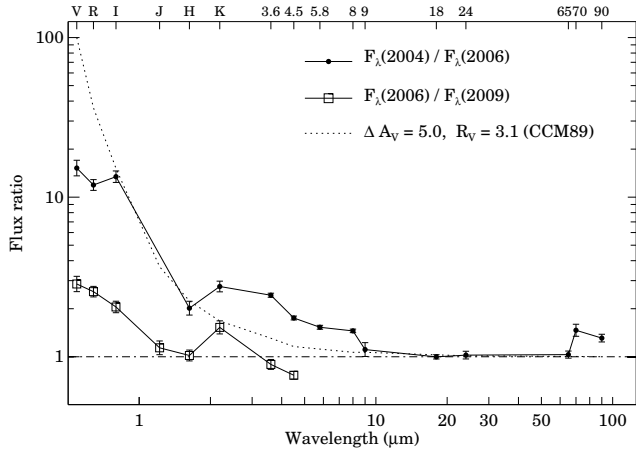


Figure 3. Flux changes of PV Cep between the different segments of the light curve, as a function of the wavelength. The dotted line shows the flux ratios corresponding to an increase of the extinction by $A_V = 5$ mag (Cardelli et al. 1989, assuming $R_V = 3.1$).

central star and various parts of the disc. The optical and near-infrared excess components are separated by a minimum in the H band. The wavelength interval 10–65 μm was unaffected by the fading, while the system also dimmed in the 70–90 μm region. The $F_\lambda(2006)/F_\lambda(2009)$ curve shows that both the star and the inner disc continued fading after the transient peak.

3.2 Variations in the nebula RNO 125

Variations in the nebula RNO 125. RNO 125 was fan-shaped and bright in the bright state (Movsessian et al. 2008), and the bright head of the cometary nebula was centered on the star (Fig. 4, upper left). A dark band appeared between the star and the nebula during the fading phase (Fig. 4, upper right). The nebula quickly faded and exhibited a strongly changing shape after the transient peak. Similar phenomenon was observed in 1977–1979 (see fig. 1 of Cohen et al. 1981). The nebula was barely visible in our images during the low-brightness phase and at the beginning of the rising phase (Fig. 4, lower left). The head of the nebula started brightening in 2010 (Fig. 4, lower right).

The variable shape of the nebula suggests that the illumination changed not only due to the fading of the star, but also due to the changing geometry of the dust distribution close to the star, resulting in rapidly changing shadows on the matter inside the outflow cavity. The rebrightening of the nebula started close to the star: those parts appeared first which dimmed when the star started declining.

3.3 Variations in the optical spectrum

No photospheric absorption lines can be identified in the spectra. With the exception of $H\alpha$, the strong emission lines are symmetric at our resolution. The forbidden lines are systematically blueshifted with respect to the permitted lines by some 100–200 km s^{-1} , indicating their origin from the approaching lobe of a wind. Table 5 shows the equivalent

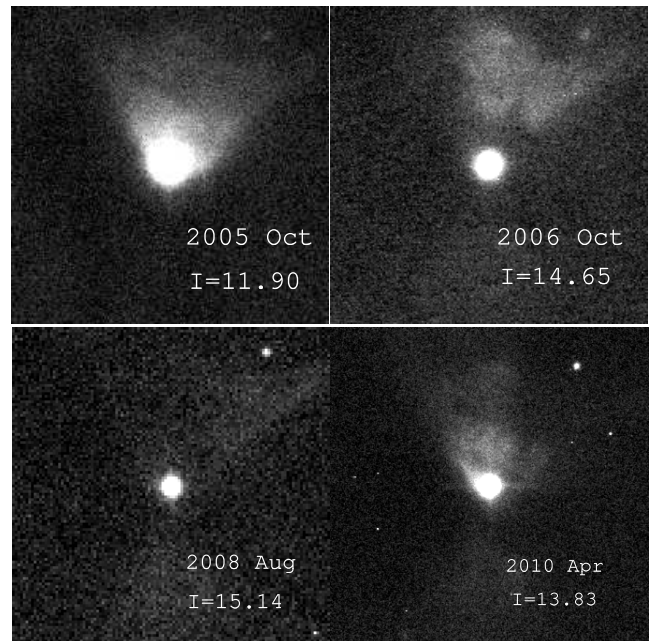


Figure 4. I-band images of the nebula RNO 125 at different dates. The size of each image is $1' \times 1'$. North is up, and east is to the right.

widths and fluxes of the strongest emission lines in the optical spectra of PV Cep, obtained in the bright, low-state, and rising phases of the light curve. The fluxes were determined using the R_C and I_C magnitudes, measured simultaneously with the spectroscopic observations, and the fluxes corresponding to zero magnitude tabulated by Glass (1999). Since only I_C magnitude is available for 2004, we estimated the R_C magnitude in 2004 using the average colour index $R_C - I_C = 1.50$, measured at the end of the bright state in 2005. The variations of the emission lines can be summarized as follows. (1) The equivalent width of the $H\alpha$ line remained nearly unchanged during the photometric decline, that is, the flux of the $H\alpha$ emission and the continuum flux underwent equal fading, suggesting that the star and the $H\alpha$ emitting region were attenuated by a circumstellar dust structure. (2) The fluxes of the forbidden lines decreased only slightly during the decline of the stellar flux (the equivalent widths strongly increased), indicating that the formation regions of these lines were unaffected by the changes leading to the fading. (3) The decline of the Ca II line fluxes was significantly larger than that of the underlying continuum: their equivalent widths were halved between 2004 and 2008. Since these lines are accretion tracers (Muzerolle, Hartmann & Calvet 1998), the accretion rate of PV Cep declined between 2004 August and 2008 August.

3.4 Physical properties of PV Cep

Mass and luminosity. Given that the amplitude of the photometric variations was smallest in the H band (Fig. 3), we estimated the luminosity of PV Cep from the H magnitude measured in the low-brightness state on 2008 June 18, assuming that the total flux in the H band originated from the photosphere. We adopted a distance of 325 pc for PV Cep (Straizys et al. 1992), an effective tempera-

Table 5. Equivalent widths and fluxes of emission lines

Id.	EW (Å)				F(10^{-17} W m^{-2})			
	2004	2008	2009	2010	2004	2008	2009	2010
H α	104	132	100	90	99	6.6	3.8	9.3
CaII 8498	77	42	62	39.5	168	4.1	6.3	11.0
CaII 8542	74	39	59	37.4	161	3.8	5.9	10.4
CaII 8662	64	32	51	30.0	139	3.1	5.1	8.3
[OI] 6300	8.1	58	82	37.0	4.8	2.9	3.1	3.8
[OI] 6363	1.7	20	27	13	1.6	1.0	1.0	1.3
[SII] 6717	1.2	4.6	9.2	3.3	1.1	0.23	0.35	0.34
[SII] 6731	1.6	8.6	15.6	5.9	1.5	0.43	0.59	0.61

ture $T_{\text{eff}} = 5500$ K, corresponding to the spectral type G8–K0 found by Magakian & Movsessian (2001)¹, a total extinction $A_V = 12.0$ mag, obtained by dereddening the near-infrared colour indices (Lorenzetti et al. 2009) on to the T Tauri locus of the $J - H$ vs. $H - K_s$ diagram (Meyer, Calvet & Hillenbrand 1997), and applied the bolometric correction tabulated by Hartigan, Strom & Strom (1994) and unreddened colour index $V - H = 1.69$ for the spectral type G8 (Kenyon & Hartmann 1995). We obtained $L_* \approx 17 L_\odot$, and a stellar radius $R_* \approx 4.0 R_\odot$. Plotting the results on the HRD, together with the evolutionary models of Palla & Stahler (1999), results in a mass of $2.4 M_\odot$ and age of < 1 Myr.

Disc accretion rates. We estimated the low-brightness-state disc accretion rate of PV Cep from the luminosity of the CaII 8542 line, measured in 2008 August (Table 5), using the empirical formula of Dahm (2008). We obtain $L_{\text{acc}}^{\text{low}} \approx 41 L_\odot$, and $\dot{M}_{\text{acc}}^{\text{low}} \approx 2.6 \times 10^{-6} M_\odot/\text{yr}$. The corresponding values for the bright state, estimated from the flux change of the CaII 8542 line, are about twice higher. The results show that the accretion rate of PV Cep is significantly higher than typical PMS accretion rates ($\sim 10^{-8} M_\odot/\text{yr}$, e.g. Gullbring et al. 1998; Dahm 2008) both in the high- and low-brightness states, and the accretion luminosity is higher than the photospheric luminosity.

4 POSSIBLE NATURE OF THE VARIATIONS

The decreased fluxes of the CaII emission lines of PV Cep between 2004 and 2008 suggest that the fading was associated with decreasing accretion rate. The factor of two drop of the accretion luminosity, derived from the CaII 8542 lines, however, can account for only $\lesssim 1$ mag variation in the optical region. To explain the whole amplitude of ~ 4 mag, enhanced circumstellar extinction also has to be invoked. The excess extinction could arise from the changes in the inner disc structure. Since $L_{\text{acc}} > L_*$, the modest drop of the

accretion rate substantially altered the total central luminosity, and the decreased central luminosity made the dust sublimation radius shrink, that is, a large amount of dust condensed in the inner disc region during the fading and the subsequent low-brightness state. The bright-state luminosity of $L_{\text{acc}} + L_* \approx 100 L_\odot$ implies $R_{\text{subl}} \sim 0.7$ AU (cf. fig. 7 of Dullemond & Monnier 2010), which might have shrunk to ~ 0.4 AU due to a factor of two drop in L_{acc} . The observed drop in the K_s -band flux between 2004 and 2007 suggests similar decrease in the dust sublimation radius, if we assume that most of this flux is emitted from the dust sublimation zone. Assuming normal interstellar gas-to-dust ratio, an excess extinction of $A_V \sim 3$ mag requires a gas column density of $\sim 6 \times 10^{21} \text{ cm}^{-2}$, which, taking into account the size of the dust condensation region, corresponds to a volume density of some 10^9 cm^{-3} . Considering typical midplane gas densities and scaleheights at the dust rim (Dullemond & Monnier 2010), the inclination of 62° and the fact that the disc of PV Cep is at least 10 times more massive than a typical HAe star disc (Hamidouche 2010), such densities along the line of sight are likely, and thus the newly formed dusty region may account for most of the observed optical and near-infrared fading of the star. The observed drop in the mid- and far-infrared fluxes indicates that parts of the optically thin outer flared disc atmosphere got into shadow.

The transient peak in 2008, according to the colour-magnitude diagrams, resulted from variable obscuration along the line of sight. A very similar transient peak both in amplitude and time-scale appeared in the light curve of PV Cep in 1979, following the end of the outburst (fig. 2 of Cohen et al. 1981), which suggests that the temporary dust-clearing might have been related to the end of the outburst. A short-lived outflow, similar to that observed in V1647 Ori after the end of its outburst in 2006, and probably associated with the rearrangement of the stellar magnetic field in response to the dropped accretion rate (Brittain et al. 2010) might have blown out some dust from the line of sight.

The slowly descending light curve accompanied by reddening between 2008 June and 2009 August may result from the dust condensation process. The duration of the low-brightness period suggests that the dust, emerging in the line of sight, was not confined to dense clumps or warps in the disc, but rather it was associated with a restructuring of the inner disc due to the changing central luminosity.

The brightening accompanied by reddening in 2009–2010 may indicate that the dust, condensed during the previous years, started evaporating. The increased CaII fluxes suggest that invigorated accretion may play role in the processes. The time-scales of the large-amplitude photometric fluctuations suggest that the inner dust rim is involved. Notably, two prominent peaks of the I_C light curve (around JD 2,455,103 and JD 2,455,143) are separated by 40 days, corresponding to the Kepler-period at a radius of 0.4 AU. The low K_s -band flux, rising fluxes at 3.6 and 4.5 μm , as well as the reappearance of the nebula suggest that the inner dust rim of the disc became less efficient in shadowing the outer parts of the circumstellar matter.

This scenario can qualitatively explain the fading in the optical, near-, mid-, and far-infrared wavelength regions, and the simultaneous variations of the nebula and the CaII emission line fluxes. Our results suggest that PV Cep differs from

¹ The widely accepted spectral type of PV Cep, A5 (Thé et al. 1994), is based on the Balmer absorption lines, observed in the spectrum at the beginning of the outburst in 1977 (Cohen et al. 1981). No spectrum, obtained after the outburst, exhibited Balmer absorption lines, which thus might have been originated from the hot inner disc in early outburst phases, even as in the case of V1057 Cyg and V1647 Ori (cf. Welin 1971; Briceño et al. 2004).

both the EXor type stars, characterized by outbursts driven by strongly enhanced accretion, and UXor stars, whose variability is caused by orbiting circumstellar dust structures. The high disc mass and persistent high accretion rate suggest that PV Cep is a protostar-like object: most of its luminosity originates from accretion, and its large-scale photometric variations reflect the changing inner disc structure, resulted from unsteady accretion. Variations in the accretion rate may be triggered by gravitational instabilities in the massive disc of PV Cep.

ACKNOWLEDGEMENTS

Our results are partly based on observations obtained at the Centro Astronómico Hispano Alemán (CAHA) at Calar Alto, operated jointly by the Max-Planck Institut für Astronomie and the Instituto de Astrofísica de Andalucía (CSIC). Our observations were supported by the OPTICON. OPTICON has received research funding from the European Community's Sixth Framework Programme under contract number RII3-CT-001566. The 0.82-m IAC-80 Telescope is operated on the island of Tenerife by the Instituto de Astrofísica de Canarias in the Spanish Observatorio del Teide. This work makes use of observations made with the *Spitzer Space Telescope*, which is operated by the Jet Propulsion Laboratory, California Institute of Technology under a contract with NASA. This publication makes use of data products from the Two Micron All Sky Survey, which is a joint project of the University of Massachusetts and the Infrared Processing and Analysis Center/California Institute of Technology, funded by the National Aeronautics and Space Administration and the National Science Foundation. This paper utilized data from the OMC Archive at LAEFF, pre-processed by ISDC. Financial support from the Hungarian OTKA grant K81966 is acknowledged. The research of Á.K. is supported by the Netherlands Organization for Scientific Research.

REFERENCES

- Acosta-Pulido J. A. et al. 2007, *AJ*, 133, 2020
 Alves J., Hartmann L., Briceño C., Lada C. J. 1997, *AJ*, 113, 1395
 Arce H. G., Goodman A. A. 2002, *ApJ*, 575, 911
 Aspin C., Beck T. L., Reipurth B. 2008, *AJ*, 135, 423
 Bibo E. A., Thé P. S. 1991, *A&AS*, 89, 319
 Briceño C. et al. 2004, *ApJ*, 606, L123
 Brittain S. D., Rettig T. W., Simon Th., Gibb E. L., Liskowsky J. 2010, *ApJ*, 708, 109
 Cardelli J. A., Clayton G. C., Mathis J. S. 1989, *ApJ*, 345, 245
 Cohen M. 1980, *AJ*, 85, 29
 Cohen M., Kuhl L. V., Harlan E. A., Spinrad H. 1981, *ApJ*, 245, 920
 Connelley M. S., Reipurth B., Tokunaga A. T. 2008, *AJ*, 135, 2496
 Cutri R. M. et al. 2003, *VizieR On-line Data Cat.: II/246*
 Dahm S. E. 2008, *AJ*, 136, 521
 Dullemond C. P., Monnier J. D. 2010, *ARA&A*, 48, 205
 Glass I. S. 1999, *Handbook of Infrared Astronomy*, Cambridge Univ. Press, p. 63
 Gómez M., Whitney B. A., Kenyon S. J. 1997, *AJ*, 114, 1138
 Grinin V. P., Arkharov A. A., Barsunova O. Yu., Sergeev S. G., Tambovtseva L. V. 2009, *Ast.Let.* 35, 114
 Gullbring E., Hartmann L., Briceño C., Calvet N. 1998, *ApJ*, 492, 323
 Gyulbudaghian A. L., Magakian T. Yu. 1977, *PAZh*, 3, 113
 Hamidouche M. 2010, *ApJ*, 722, 204
 Hartigan P., Strom K. M., Strom S. E. 1994, *ApJ*, 427, 961
 Herbig G. H. 1989, in Reipurth B., ed., *ESO Workshop on Low Mass Star Formation and Pre-Main Sequence Objects*, ESO: Garching, p. 233
 Hora J. L. et al. 2008, *PASP*, 120, 1233
 Ishihara D. et al. 2010, *A&A*, 514, A1
 Kenyon S. J., Hartmann L. 1995, *ApJS*, 101, 117
 Kóspál Á., Ábrahám P., Apai D., Ardila D. R., Grady C. A., Henning Th., Juhász A., Miller D. W., Moór A. 2008, *MNRAS*, 383, 1015
 Kun M., Balog Z., Kenyon S. J., Mamajek E. E., Guter-muth R. A. 2009, *ApJS*, 185, 451
 Levreault R. M. 1984, *ApJ*, 277, 634
 Lorenzetti D., Larionov V. M., Giannini T., Arkharov A. A., Antonucci S., Nisini B., Di Paola A. 2009, *ApJ*, 693, 1056
 Lu N. et al. 2008, *PASP*, 120, 328
 Magakian T. Yu., Movsessian T. A. 2001, *Astrophys.*, 44, 419
 Meyer M. R., Calvet N., Hillenbrand L. A. 1997, *AJ*, 114, 288
 Movsessian T. A., Magakian T. Yu., Sargsyan D. M., Nikogossian E. H. 2008, *Astrophysics*, 51, 387
 Muzerolle J., Hartmann L., Calvet N. 1998, *AJ*, 116, 2965
 Neckel T., Staude H. J., Sarcander M., Birkle K. 1987, *A&A*, 175, 231
 Pál A. 2009, PhD Thesis, Eötvös Loránd University, Budapest (arXiv:0906.3486)
 Palla F., Stahler S. W. 1999, *ApJ*, 525, 772
 Reipurth B., Bally J., Devine D. 1997, *AJ*, 114, 2708
 Stetson P. B. 2000, *PASP*, 112, 925
 Straizys V., Cernis K., Kazlauskas A., Meistas E. 1992, *Balt. Astr.*, 1, 149
 Thé P. S., de Winter D., Pérez M. R. 1994, *A&AS*, 104, 315
 Welin G. 1971, *A&A*, 12, 312
 Yamamura I., Makiuti S., Ikeda N., Fukuda Y., Oyabu S., Koga T., White G. J. 2010, *AKARI-FIS BSC Release note Version 1.0*, ISAS/JAXA
 Zhu Z., Hartmann L., Gammie C., McKinney J. C. 2009, *ApJ*, 701, 620

ONLINE SUPPORTING MATERIAL

APPENDIX A: SPITZER DATA REDUCTION

IRAC. The IRAC observations of PV Cep were performed in two different observing modes. The observations in 2004 and those in the framework of the post-Helium monitoring programme were performed using the subarray readout mode. The observations in 2006 were performed in high dynamic range readout mode with 0.6 s and 12 s integration time.

The subarray mode allows the utilization of exposure time as short as 0.02 s enabling the observation of bright sources that would saturate the detector using the other readout modes. The data processing was started from the *Spitzer* Science Center (SSC) basic calibrated data (BCD)

produced by the pipeline version S18.7. The BCD image cubes of the 64 frames were combined into two-dimensional images using the “irac-subcube-collapse” IDL routine provided by the SSC. The observation performed in 2004 was made of nine different dither positions and repeated three times resulting in 27 images at each wavelength. In the case of monitoring observations four dithering steps were utilized, leading to four images at each wavelength. We performed aperture photometry on the final images at each wavelength using a modified version of the IDLPHOT routines. The aperture radius was set to 3 pixels, the sky background was computed in an annulus with an inner radius of 3 pixels and a width of 4 pixels. In the course of the sky estimates we used an iterative sigma-clipping method, where the clipping threshold was set to 3σ . Following the outline of Hora et al. (2008) we also applied an array-dependent photometric correction and a pixel-phase correction to the measured flux densities. An aperture correction was then performed using the values published in the IRAC Data Handbook. The individual flux density values measured in the different dither positions (at each band) were averaged to get the final photometry. The measurement error was estimated as the r.m.s. of the individual flux densities.

In the case of the high dynamic range mode observations, we made the photometry on individual saturation corrected, CBCD, images. Because of the bright target we used only those 12 short exposure time images (with integration time of 0.6 s) where PV Cep appeared on the frames. In the course of photometry we used the same method as in the case of subarray mode observations.

The final uncertainties of the photometry were computed by adding quadratically the measurement errors and an absolute calibration error of 2% (IRAC Data Handbook).

IRS. The *Spitzer* spectroscopic observations of PV Cep were obtained in spectral mapping mode with the short low (5.2–14.5 μm , $R\approx 60$ –127), short high (9.9–19.5 μm , $R\approx 600$), and long high (18.7–37.2 μm , $R\approx 600$) channels. The spectral maps consisted of two nod positions and nine positions perpendicular to the slit. We only considered the two central positions, as if it were a normal staring measurement. The data were processed at the SSC with the S18.7.0 pipeline to BCD level. We extracted spectra from the two-dimensional dispersed BCD images using the *Spitzer* IRS Custom Extraction software (SPICE version 2.1.2). In the case of the short low channel, we first subtracted the two nod positions from each other in order to remove the sky background, then extracted a spectrum from a wavelength-dependent, tapered aperture around the star. In the case of the high-resolution channels, we extracted spectra from the full slit. Since no extended emission could be detected in the IRAC images, we calibrated the spectra by assuming that PV Cep is a point source. In case the star was not well centered in the slit (i.e. the offset from the slit center perpendicular to the slit was $\geq 0.5''$), we corrected the spectra for flux loss using the measured IRS beam profiles, following the procedure described in Kóspál et al. (2008). After this, there was still a slight mismatch between the different channels. The discrepancy could be eliminated by simply adding a linear correction to the short high channel.

MIPS photometry. 24 and 70 μm images of PV Cep were obtained as part of the Gould Belt Legacy Survey. We started from BCD files reduced with the *SSC* pipeline version S16.1. At 70 μm , we used GeRT (version S14.0 v1.1 [060415]) to do column mean subtraction and time filtering on the BCD files. We used MOPEX (version 18.1.5) to create mosaics at both 24 and 70 μm , with pixel scales of 2.45'' and 4'', respectively. Since PV Cep was saturated at both wavelengths, aperture photometry was not possible. In order to determine the flux of PV Cep, we first obtained aperture photometry for 7 or 5 non-saturated stars in the field at 24 and 70 μm , respectively, (an aperture radius of 7'', sky annulus between 40 and 50'', and aperture correction of 1.61 was used at 24 μm , and an aperture radius of 8'', sky annulus between 39 and 65'', and aperture correction of 3.70 was used at 70 μm). Then we normalized the psf profiles of these stars to 1 Jy and averaged them. The obtained psf profile was then fitted to the non-saturated parts of the profile of PV Cep and the scaling factor needed for a good fit directly gave the flux of our target.

MIPS spectroscopy. The low resolution far-IR (55–95 μm , $R\approx 15$ –25) spectrum of PV Cep was obtained in the MIPS spectral energy distribution (SED) mode. Two observing cycles were performed, each consisting of six pairs of 3 s long on- and off-source exposures. The on-source and the background position was separated by 1'. The data reduction of the MIPS SED observation was started with the BCD images (pipeline version S18.12) and the MOPEX software was utilized to perform the necessary processing steps (combination of data, background removal, application of dispersion solution) and to compile the final image with pixel size of 9.8''. The spectrum was extracted from the sky-subtracted final image using a five pixel wide aperture. As a final step an aperture correction was applied, the aperture correction factors were taken from Lu et al. (2008).

Table A1. Comparison stars

N	RA(2000) h m s	D(2000) d ' ''	V(ΔV) [mag]	R_C (ΔR_C) [mag]	I_C (ΔI_C) [mag]
C1	20 46 28.89	+67 59 05.4	14.072 (0.012)	13.595 (0.012)	13.200 (0.008)
C2	20 46 26.50	+67 58 11.8	14.608 (0.005)	13.948 (0.004)	13.495 (0.005)
C3	20 46 10.44	+67 55 44.2	15.134 (0.005)	14.205 (0.004)	13.637 (0.004)
C4	20 46 01.22	+67 55 26.7	16.741 (0.010)	15.654 (0.005)	14.670 (0.004)
C5	20 45 48.42	+67 59 12.2	15.125 (0.008)	14.505 (0.005)	14.000 (0.005)
C6	20 46 37.77	+67 58 58.4	15.648 (0.008)	14.907 (0.005)	14.289 (0.005)
C7	20 45 41.29	+67 59 28.0	16.747 (0.015)	16.074 (0.012)	15.538 (0.007)
C8	20 45 46.21	+67 55 25.3	17.969 (0.015)	16.812 (0.012)	15.712 (0.008)
C9	20 46 22.32	+67 54 56.2	15.676 (0.010)	14.938 (0.008)	14.363 (0.007)
C10	20 46 28.89	+67 55 30.5	16.945 (0.010)	16.366 (0.010)	15.877 (0.007)
C11	20 46 36.19	+67 55 54.7	16.210 (0.010)	15.739 (0.010)	15.345 (0.007)
C12	20 46 25.74	+67 56 54.0	16.190 (0.010)	15.538 (0.006)	15.009 (0.006)
C13	20 46 22.09	+67 59 16.9	16.480 (0.010)	15.835 (0.006)	15.304 (0.008)
C14	20 46 19.98	+67 59 53.4	16.163 (0.010)	15.631 (0.005)	15.212 (0.005)
C15	20 46 37.26	+67 57 41.1	14.676 (0.005)	14.105 (0.005)	13.649 (0.007)
C16	20 45 43.02	+67 59 00.1	15.723 (0.009)	14.995 (0.005)	14.412 (0.007)

Table A2. Results of the photometry of PV Cep

JD (2454000+)	Date yyyymmdd	$V(\Delta V)$ mag	$R_C(\Delta R_C)$ mag	$I_C(\Delta I_C)$ mag	Telescope
-329	20051027	14.58 (0.16)	13.28 (0.06)	11.78 (0.06)	RCC
-327	20051029	15.08 (0.04)	13.39 (0.04)	11.90 (0.11)	RCC
-326	20051030	15.43 (0.06)	13.59 (0.04)	11.98 (0.06)	RCC
-325	20051031	15.14 (0.07)	13.36 (0.01)	11.84 (0.16)	RCC
-308	20051117	15.59 (0.04)	13.76 (0.05)	12.34 (0.05)	RCC
1	20060922	17.46 (0.05)	15.98 (0.02)	14.60 (0.02)	RCC
26	20061017	17.54 (0.05)	15.98 (0.02)	14.65 (0.02)	RCC
570	20080413	...	15.36 (0.05)	13.60 (0.04)	Schmidt
589	20080502	14.11 (0.02)	Schmidt
594	20080507	14.25 (0.04)	Schmidt
626	20080608	14.99 (0.02)	Schmidt
627	20080609	...	16.39 (0.02)	15.03 (0.02)	Schmidt
645	20080627	...	16.55 (0.02)	15.12 (0.03)	RCC
646	20080628	...	16.57 (0.02)	15.14 (0.04)	RCC
647	20080629	...	16.61 (0.01)	15.16 (0.01)	RCC
649	20080701	...	16.70 (0.01)	15.21 (0.01)	RCC
650	20080702	...	16.61 (0.03)	15.20 (0.02)	RCC
675	20080727	...	16.74 (0.04)	15.33 (0.04)	Schmidt
676	20080728	...	16.82 (0.04)	15.43 (0.04)	Schmidt
693	20080814	...	16.67 (0.01)	15.31 (0.01)	Schmidt
705	20080826	18.37 (0.03)	16.69 (0.03)	15.09 (0.04)	CA 2.2-m
707	20080828	15.15 (0.02)	Schmidt
708	20080829	18.04 (0.03)	16.50 (0.03)	15.14 (0.03)	CA 2.2-m
709	20080830	15.02 (0.02)	Schmidt
710	20080831	...	16.35 (0.02)	15.00 (0.02)	Schmidt
738	20080928	17.80 (0.02)	16.32 (0.01)	15.00 (0.01)	RCC
757	20081017	17.94 (0.03)	16.41 (0.03)	15.07 (0.03)	RCC
758	20081018	17.75 (0.02)	16.29 (0.01)	14.94 (0.01)	RCC
760	20081020	17.81 (0.02)	16.35 (0.01)	15.00 (0.01)	RCC
782	20081111	14.94 (0.01)	Schmidt
808	20081207	...	16.24 (0.04)	14.84 (0.05)	Schmidt
809	20081208	...	16.19 (0.02)	14.80 (0.02)	Schmidt
840	20090108	15.18 (0.02)	Schmidt
841	20090109	18.08 (0.10)	16.54 (0.07)	15.22 (0.04)	Schmidt
883	20090220	...	16.84 (0.05)	15.41 (0.06)	Schmidt
892	20090224	15.34 (0.04)	Schmidt
912	20090321	15.11 (0.03)	Schmidt
916	20090325	...	16.58 (0.04)	15.24 (0.04)	Schmidt
947	20090425	...	16.88 (0.01)	15.38 (0.01)	Schmidt
949	20090427	...	16.74 (0.01)	15.31 (0.01)	Schmidt
950	20090428	...	16.62 (0.02)	15.24 (0.01)	Schmidt
951	20090429	...	16.79 (0.02)	15.33 (0.01)	Schmidt
953	20090501	...	16.79 (0.02)	15.28 (0.02)	RCC
972	20090520	...	16.97 (0.01)	15.50 (0.01)	RCC
974	20090522	...	16.97 (0.01)	15.48 (0.01)	Schmidt
976	20090524	...	16.35 (0.03)	15.19 (0.02)	Schmidt
978	20090526	...	16.85 (0.02)	15.43 (0.02)	Schmidt
1001	20090618	...	16.91 (0.04)	15.44 (0.05)	RCC
1022	20090709	...	16.91 (0.04)	15.45 (0.03)	Schmidt
1027	20090714	...	16.95 (0.04)	15.49 (0.04)	Schmidt
1058	20090814	...	17.23 (0.02)	15.70 (0.02)	Schmidt
1060	20090816	...	17.24 (0.01)	15.70 (0.02)	Schmidt
1061	20090817	...	17.27 (0.01)	15.71 (0.02)	Schmidt
1062	20090818	...	17.37 (0.01)	15.86 (0.02)	Schmidt
1071	20090827	...	17.39 (0.01)	15.78 (0.01)	RCC
1072	20090828	...	17.40 (0.01)	15.77 (0.01)	RCC

Table A2. Results of the photometry of PV Cep (cont.)

JD (2454000+)	Date yyyymmdd	V_C (ΔV_C) mag	R_C (ΔR_C) mag	I (ΔI) mag	Telescope
1077	20090902	15.48 (0.01)	RCC
1093	20090918	...	16.95 (0.02)	15.21 (0.02)	RCC
1094	20090919	...	16.93 (0.02)	15.10 (0.02)	RCC
1095	20090920	...	16.87 (0.02)	15.17 (0.02)	RCC
1096	20090921	...	16.91 (0.02)	15.17 (0.02)	RCC
1101	20090926	18.24 (0.06)	16.59 (0.01)	14.93 (0.01)	RCC
1103	20090928	...	16.46 (0.02)	14.73 (0.01)	Schmidt
1113	20091008	...	17.05 (0.03)	15.35 (0.03)	Schmidt
1114	20091009	18.69 (0.04)	16.95 (0.01)	15.32 (0.01)	CA 2.2-m
1115	20091010	...	16.96 (0.04)	15.48 (0.06)	Schmidt
1116	20091011	18.70 (0.04)	17.00 (0.03)	15.33 (0.03)	CA 2.2-m
1119	20091014	18.60 (0.01)	16.83 (0.01)	15.12 (0.01)	CA 2.2-m
1130	20091025	...	16.85 (0.02)	15.08 (0.02)	IAC-80
1137	20091101	18.18 (0.04)	16.61 (0.02)	14.66 (0.01)	IAC-80
1139	20091103	...	16.54 (0.02)	14.59 (0.02)	IAC-80
1140	20091104	...	16.59 (0.02)	14.73 (0.02)	IAC-80
1142	20091106	18.21 (0.04)	16.39 (0.02)	14.46 (0.02)	IAC-80
1143	20091107	18.08 (0.03)	16.40 (0.02)	14.45 (0.02)	IAC-80
1149	20091113	...	16.51 (0.03)	14.58 (0.04)	Schmidt
1155	20091119	...	16.95 (0.04)	15.33 (0.04)	Schmidt
1156	20091120	...	16.72 (0.03)	15.12 (0.03)	Schmidt
1159	20091123	...	16.95 (0.01)	15.35 (0.02)	Schmidt
1161	20091125	...	16.98 (0.01)	15.32 (0.01)	Schmidt
1212	20100115	...	16.45 (0.05)	14.53 (0.06)	Schmidt
1213	20100116	...	16.37 (0.06)	14.46 (0.07)	Schmidt
1253	20100225	...	16.27 (0.13)	14.56 (0.12)	Schmidt
1259	20100303	...	16.36 (0.13)	14.38 (0.12)	Schmidt
1288	20100401	...	15.55 (0.07)	13.76 (0.05)	Schmidt
1295	20100408	...	15.87 (0.01)	13.83 (0.05)	RCC
1331	20100514	...	15.50 (0.02)	13.56 (0.02)	RCC
1372	20100624	17.70 (0.06)	15.81 (0.03)	14.02 (0.03)	Schmidt
1420	20100812	17.45 (0.01)	15.53 (0.01)	13.64 (0.01)	RCC
1435	20100826	...	16.19 (0.04)	14.31 (0.05)	Schmidt
1461	20100921	...	15.58 (0.03)	13.53 (0.03)	RCC
1463	20100923	...	15.90 (0.05)	14.06 (0.04)	Schmidt
1464	20100924	...	15.86 (0.05)	13.99 (0.06)	Schmidt
1477	20101007	14.13 (0.03)	Schmidt
1524	20101123	...	16.15 (0.04)	14.45 (0.04)	Schmidt

Table A3. *Spitzer* photometry for PV Cep. All fluxes are color-corrected and given in Jy.

Date	$F_{3.6\mu\text{m}}$	$F_{4.5\mu\text{m}}$	$F_{5.7\mu\text{m}}$	$F_{8.0\mu\text{m}}$	$F_{24\mu\text{m}}$	$F_{70\mu\text{m}}$
20041029	4.47 (0.09)	6.98 (0.14)	8.34 (0.17)	11.85 (0.23)		
20061126	1.84 (0.04)	3.99 (0.08)	5.45 (0.11)	8.16 (0.17)		
20070226					27.12 (1.04)	35.22 (2.13)
20090916	3.54 (0.03)	5.97 (0.02)				
20090917	3.16 (0.03)	5.41 (0.03)				
20090918	3.19 (0.07)	5.31 (0.03)				
20090919	3.31 (0.03)	5.48 (0.03)				
20090920	3.22 (0.02)	5.34 (0.02)				
20090921	3.11 (0.04)	5.19 (0.04)				
20090922	3.29 (0.04)	5.40 (0.03)				
20100109	3.27 (0.07)	5.53 (0.03)				
20100110	3.14 (0.04)	5.31 (0.02)				
20100111	3.31 (0.05)	5.49 (0.02)				
20100112	3.34 (0.08)	5.67 (0.02)				
20100113	3.26 (0.04)	5.46 (0.03)				
20100114	3.00 (0.08)	5.16 (0.02)				
20100115	3.05 (0.02)	5.23 (0.02)				